



**HAL**  
open science

# Experimental Determination of the Geometry of Real Drops on Transparent Materials

J. Pieters, J. Deltour, M. Debruyckere

► **To cite this version:**

J. Pieters, J. Deltour, M. Debruyckere. Experimental Determination of the Geometry of Real Drops on Transparent Materials. *Journal de Physique III*, 1996, 6 (7), pp.975-989. 10.1051/jp3:1996166 . jpa-00249503

**HAL Id: jpa-00249503**

**<https://hal.science/jpa-00249503>**

Submitted on 4 Feb 2008

**HAL** is a multi-disciplinary open access archive for the deposit and dissemination of scientific research documents, whether they are published or not. The documents may come from teaching and research institutions in France or abroad, or from public or private research centers.

L'archive ouverte pluridisciplinaire **HAL**, est destinée au dépôt et à la diffusion de documents scientifiques de niveau recherche, publiés ou non, émanant des établissements d'enseignement et de recherche français ou étrangers, des laboratoires publics ou privés.

# Experimental Determination of the Geometry of Real Drops on Transparent Materials

J.G. Pieters (<sup>1,\*</sup>), J.M. Deltour (<sup>2</sup>) and M.J. Debruyckere (<sup>1</sup>)

(<sup>1</sup>) University of Ghent, Department of Agricultural Engineering, Coupure Links 653, 9000 Gent, Belgium

(<sup>2</sup>) Faculté Universitaire des Sciences Agronomiques de Gembloux, UER de Physique et de Chimie Physique, Avenue de la Faculté 8, 5030 Gembloux, Belgium

(Received 21 December 1995, revised 1 April 1996, accepted 16 April 1996)

PACS.42.15.Gs – Geometrical Optics - Other topics

PACS.42.25.Fx – Wave Optics - Diffraction and Scattering

PACS.42.30.Yc – Imaging and Optical processing - Other topics

**Abstract.** — An experimental method for the determination of real drop geometries on transparent supports is developed. The method offers the possibility to obtain the general form of a drop by using commonly available instruments, such as a photo camera with bellow, a digitizer or a scanner. By means of this method, a set of isoclinal lines of the drop is registered by a camera. By integration, the map of isoclinal lines is then mathematically transformed into a relief-map of the drop, revealing all geometric information about the drop profile. A trial and error method for the correction of the measuring equipment alignment errors is also developed. For a series of 15 drops on a vertical PE film and whose geometries are determined by means of the above mentioned method, light transmission and diffusion are then simulated. It is shown that the light transmittance of flat drops is somewhat lower than the light transmittance for dry PE but much higher than for hemispherical drops. Light diffusion is shown to be nearly independent of the drop shape. Nearly all the light is diffused in a small solid angle. For an evaporating drop on a vertical PE film, the evolutions of the drop geometry and the light transmittance are followed in time. It is also demonstrated that during evaporation, the drop becomes mainly flatter so that the light transmittance increases.

## 1. Introduction

There are very few methods described in literature allowing for the determination of the geometries of real drops, because of the difficulties arising from the transparency and the small size of the drops. In this paper, a method developed for the study of condensation drops on glass and plastic walls and roofs of greenhouses, will be presented. Therefore, this method must meet several requirements. Of course the method must be cheap. This implies that only commonly available materials and apparatus can be used. The determination of drop geometry must be executable under several circumstances: in the laboratory as well as *in situ*, i.e. a greenhouse or an other location where condensation occurs. Another important requirement is

---

(\*) Author for correspondence (e-mail: Jan.Pieters@rug.ac.be)

that the recording of the drop geometry should ask a very short time. Otherwise, deformations are to be expected, due to growth of the drop by condensation or to shrinkage by evaporation.

By means of this method, the geometries of 15 drops, sprayed on a vertical PE film, will be determined and input in a simulation program, allowing for the determination of the light transmittance and diffusion of these drops. Furthermore, the geometry of an evaporating drop will be determined at 5 minutes intervals to investigate the influence of evaporation on light transmittance.

## 2. Literature Review

2.1. THEORETICAL APPROACHES. — Since the 19<sup>th</sup> century, a lot of authors have tried to study the wettability of materials and to determine drop shapes in a theoretical way. A state of the art in this field can be found in *e.g.* [1] and [2]. Most attempts to describe the drop profile mathematically, however, were unsuccessful. Using the Laplace equation, equations for the description of the three-dimensional profiles of drops lying on horizontal, inclined and vertical plates, were obtained by [3]. But this treatment revealed itself unable to picture the experimental behaviour of the droplets. A more frequently met starting-point is the fact that a drop adopts the shape characterized by minimal potential energy. However, as far as we know, only numerical solutions for a drop on a horizontal surface (*e.g.* [4]) and for infinitely broad drops on a vertical surface [5] are mentioned in literature.

2.2. EXPERIMENTAL APPROACHES . — As for each solid-liquid interaction in the air, there is only one contact angle  $\theta$ , defined by the well-known Young equation, one might think of editing an empirical relationship between the drop profile and the contact angle, which can be measured accurately and easily. However, as the Young equation does not include the influence of gravitation, it is only valid for small droplets. Moreover, the contact angle gives only a local indication at the triple contact line. Furthermore, due to surface roughness [6] and other surface irregularities (which are not yet all known), drops on an inclined solid do not have a unique contact angle  $\theta$ , so that local contact angles may vary between the so-called advancing and receding contact angles  $\theta_A$ , respectively  $\theta_R$ . It should be clear from this that the above mentioned experimental formulas would be too specific or too complicated for practical use.

As the forming of a simple mathematical equation based on a few experimentally determined characteristics of the fluid and the solid seems to be impossible and since such formulas could never describe the enormous variety of drops that can be observed on a same support and under the same circumstances, some authors have directly measured droplet profiles or parts of it. Tanner described a few simple methods. Using a refractometer, he was able to get a kind of relief-map of very flat drops [7]. Since the dark and bright lines of the interferogram, resulting from the reflections on the interfaces plate-liquid and liquid-vapour of the drop, are to be considered as lines of equal drop height with a constant interval which can be expressed as a function of the index of refraction of the fluid and the wavelength of the light, the drop profile can be described numerically.

In the case of very flat drops, the height interval  $\Delta\xi$  between two fringes can easily be demonstrated to be given by

$$\Delta\xi = \frac{\lambda}{2n_d} \quad (1)$$

with  $\lambda$  : wave length of the light [m]  
 $n_d$  : refractive index of the drop fluid [-].

Using a classical HeNe-laser as the coherent light source with a wavelength of 632.8 nm, each fringe stands for a 226 nm height interval.

This method, although rather easy to build, has an important disadvantage: it can only be used for very flat drops. Otherwise, the number of fringes becomes very high. For strongly curved drops, light rays can be totally reflected if the angle of incidence at the water-air interface of the drop exceeds the limit angle. In the case of a reflection interferometer (where the parallel light rays are reflected on the air-water interface of the droplets) the light rays are scattered in nearly all directions. For drops having important curvatures, an other method is to be sought.

### 3. Method for Extremely Curved Drops

3.1. PRINCIPLE. — The principle of such a method for drops with “extreme” contact angles, was again suggested by Tanner [8]. A regular pattern (*e.g.* a series of concentric circles) is drawn on a computer monitor. The drop, acting like a lens with a short focal length, collects light rays with different directions issued from the target and forms an image at infinite distance by emerging rays parallel to the optical axis. If the target pattern is known, its picture through the lens can give information about the drop geometry. Tanner adopted that for small contact angles, there is a linear relationship between the target ring radius  $R$  on the monitor screen and the slope angle  $\eta$  of the drop at the point from which the concerned light rays emerge parallel to the optical axis, given by

$$\Delta\eta \approx \frac{n_a}{n_d - n_a} \left( \frac{\Delta R}{l_1} \right) \quad (2)$$

where  $n_a$  and  $n_d$  are the absolute refractive indexes for air and for the drop fluid and where  $l_1$  is the distance between the screen and the drop. It is somewhat surprising that Tanner adopted a formula which is only valid for small angles, although he was looking for a “deflection mapping technique with extreme angular range”. As condensation drops on *e.g.* PE can have extremely large contact angles, this method will be further developed. In the following paragraphs, a method that is valid for convex drops with any contact angle up to 90° and based on the same principle, will be given. It will also be shown that equation (2) can be obtained as a special case of the formulas developed there.

### 3.2. IMPROVEMENT OF THE METHOD

3.2.1. *Non-Linearity of the Slope Equation.* — Figure 1 shows the deflections of a light ray, starting from a point on the screen, passing through a slab or film, entering a convex drop and leaving it parallel to the optical axis at a point where the slope of the drop surface equals  $\eta$ . It is supposed that the object distance of the camera is set at  $\infty$ .

With the notations of Figure 1 and by applying the well-known Snellius-Descartes law, it can be deduced from the figure that:

$$n_a \sin(\varphi_1) = n_p \sin(\varphi_2) = n_d \sin(\varphi_3) \quad (3)$$

and

$$n_a \sin(\eta) = n_d \sin(\varphi_4) \quad (4)$$

The angles  $\varphi_2$ ,  $\varphi_3$  and  $\varphi_4$  can then be expressed as a function of the known incidence angle  $\varphi_1$  or the slope angle  $\eta$ , which is the unknown to be determined.

$$\varphi_2 = \arcsin \left( \frac{n_a}{n_p} \sin(\varphi_1) \right) \quad (5)$$

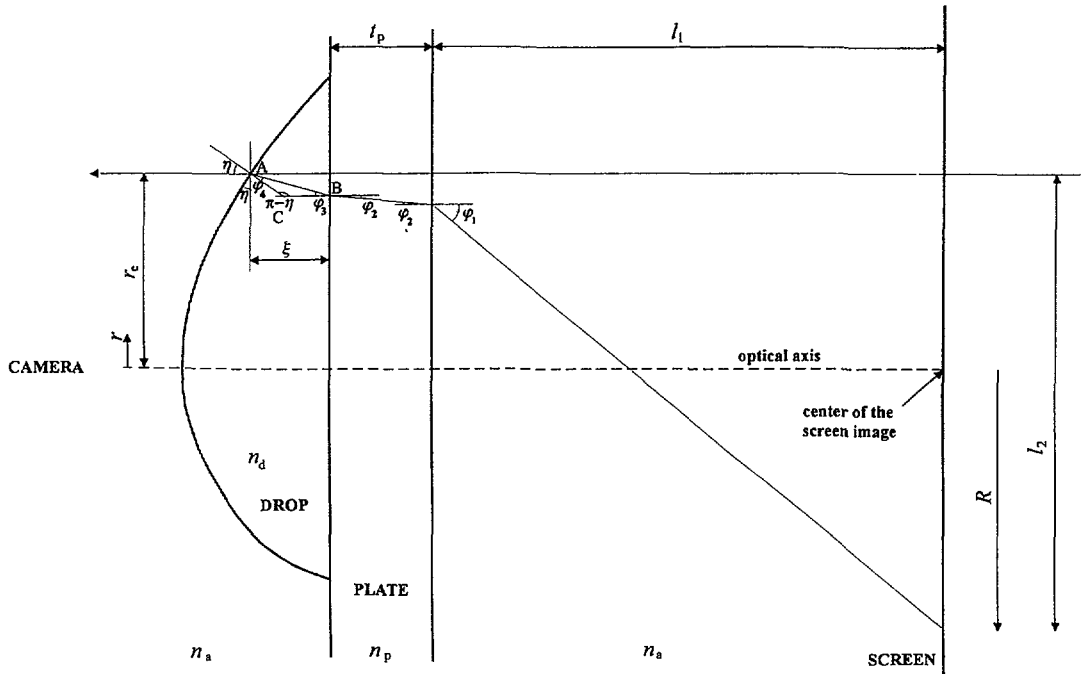


Fig. 1. — Scheme for the development of the slope and height formulas of the drop (symmetry plane).

$$\varphi_3 = \arcsin\left(\frac{n_a}{n_d} \sin(\varphi_1)\right) \tag{6}$$

$$\varphi_4 = \arcsin\left(\frac{n_a}{n_d} \sin(\eta)\right). \tag{7}$$

For the triangle ABC of Figure 1, it holds that:

$$(\pi - \eta) + \varphi_3 + \varphi_4 = \pi \tag{8}$$

By rearranging and by substituting equations (6) and (7), equation (8) can be transformed into

$$-\eta + \arcsin\left(\frac{n_a}{n_d} \sin(\varphi_1)\right) + \arcsin\left(\frac{n_a}{n_d} \sin(\eta)\right) = 0. \tag{9}$$

The incidence angle  $\varphi_1$  can now be expressed as an explicit function of the slope angle  $\eta$ :

$$\varphi_1 = \arcsin\left(\frac{n_d}{n_a} \sin\left(\eta - \arcsin\left(\frac{n_a}{n_d} \sin(\eta)\right)\right)\right) \tag{10}$$

which is clearly unlinear. However, for small incidence angles and for small slope angles, the sines and arcsines can be approximated by the angles themselves, so that in this case equation (10) reduces to

$$\eta = \frac{n_a}{n_d - n_a} \varphi_1, \tag{11}$$

which is the integrated version of the linear approximation of equation (2) used in reference [8].

3.2.2. Height Equation

3.2.2.1. Symmetry Planes. — Until now, only the direction of the rays and the slope of the drop surface were taken into account. The deformation of the screen image by the drop, however, also depends on the drop height. In the scheme of Figure 1, the optical axis of the camera contains the top of the drop (where  $\eta = 0$ ) and the center of the screen image for a symmetry plane of a drop. Be  $R$  the distance from any point on the screen to the center of the screen image. From this point, a light ray, having an incidence angle  $\varphi_1$ , leaves towards the slab and the drop, where it is refracted in a direction, parallel to the optical axis at a distance  $r_e$ . Be  $l_2$  the distance from the point on the screen to the orthogonal projection of the point where the ray leaves the drop. The distance  $R$  can then simply be expressed as the difference between these two distances:

$$R = l_2 - r_e \tag{12}$$

By means of some simple geometry, the expression of  $l_2$  as a function of the angles  $\varphi_1, \varphi_2, \varphi_3$ , the drop thickness  $\xi$  at the emergence point of the light ray, the plate thickness  $t_p$  and the distance  $l_1$  between the screen and the plate can be deduced from Figure 1.

$$l_2 = \xi \tan(\varphi_3) + t_p \tan(\varphi_2) + l_1 \tan(\varphi_1). \tag{13}$$

By substituting equations (5) and (6) in equation (13) and then equation (13) in equation (12),  $R$  can be expressed as

$$R = \xi \tan \left( \arcsin \left( \frac{n_a}{n_d} \sin(\varphi_1) \right) \right) + t_p \tan \left( \arcsin \left( \frac{n_a}{n_p} \sin(\varphi_1) \right) \right) + l_1 \tan(\varphi_1) - r_e. \tag{14}$$

Since the expression of  $\varphi_1$  as a function of the slope angle  $\eta$  is known (See Eq. (10)), there are only two unknowns in this equation: the slope angle  $\eta$  and the height  $\xi$  of the drop. This means that another equation is to be found for the total determination of the drop geometry. Since the drop height is known to be 0 at the edge of the drop and since

$$d\xi = \tan(\eta)dr, \tag{15}$$

where  $\eta$  is a function of  $r$ , it is clear that for each radial plane that contains the optical axis, the following can be written:

$$\xi(r) = \int_0^{r_e} \tan(\eta)dr. \tag{16}$$

In finite difference form, equation (16) becomes

$$\xi_n = \xi_{n-1} + \tan(\eta)\Delta r, \tag{17}$$

where  $\xi_0 = 0$  and where  $n$  is a positive integer.

3.2.2.2. Other than Symmetry Planes. — For asymmetric drops, the plane containing the axis through the center of the target and through the top of the drop (perpendicular to the plane of the target and coinciding with the optical axis of the camera) and the plane containing the incident and the outgoing light ray at the point where the light ray leaves the drop, not necessarily coincide but include an angle  $\gamma$ . Since in that case  $r_e$  and  $R$  are no longer coplanar, equation (12) and consequently equation (14) are no longer valid. A scheme of this situation, projected in the plane of the target, is given in Figure 2.

From this figure, it is found that for other than symmetry planes, equation (12) should be replaced with

$$R = \sqrt{l_2^2 + r_e^2 - 2l_2r_e \cos \gamma}. \tag{18}$$

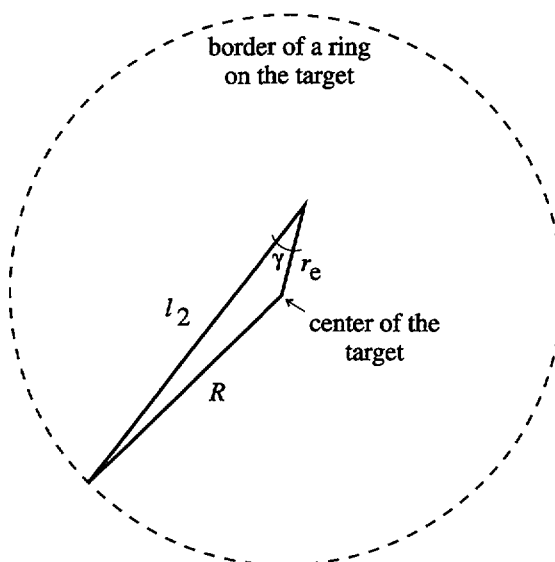


Fig. 2. — Projection of  $R$  and  $r_e$  in the plane of the target.

Since the drop shape is to be determined, the angle  $\gamma$  is not known. For most cases, however,  $r_e$  is very small when compared to  $R$ . For normal drops,  $r_e$  is of the order of a few mm, while  $R$  is of the order of several cm. Furthermore, for commonly met drop shapes  $\gamma$  will be rather small so that equation (12) can be considered as a good approximation for equation (18). A numerical estimation of the difference between the results obtained by means of equations (12) and (18) is given in Annex for a hypothetical drop shape.

**3.2.3. Calculation of the Drop Height.** — The system of equations (10), (14) and (17) can now be solved iteratively. In this way the height of the drop can be calculated in several points, lying in several planes, which all contain the optical axis of the camera. For any of these points, it suffices to measure (and rescale)  $r_e$  so that by means of the above mentioned equations the corresponding set of values for  $\varphi_1$ ,  $\eta$  and  $\xi$  can be found. For a correct application of the method described above, it is necessary that the center of the image on the screen and the top of the drop lie on the optical axis of the camera. In that case, the center of the screen seen through the drop would coincide with the center that is directly seen. In practice, it is not always possible to align all these elements. Corrections are then to be carried out. These will be dealt with in the practical implementation of the method.

### 3.3. IMPLEMENTATION OF THE METHOD

**3.3.1. Recording of the Drop Geometry.** — For the determination of the drop geometry, the experimental unit shown in Figure 3, was built. In the following paragraphs, each of the elements will be discussed in some more detail.

**3.3.1.1. Light Source and Target.** — Instead of drawing circular rings of equal width, rings with varying widths were chosen. This kind of "target" offered the great advantage that the top - which is mostly flat - as well as the border region of the drops - which is mostly strongly curved -, could be studied under optimal conditions. The widths of the rings were chosen so that each one covered a slope angle range  $\Delta\eta$  of  $5^\circ$  according to equation (10). By this

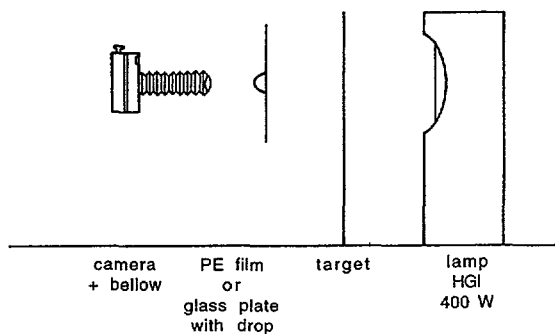


Fig. 3. — Experimental unit for the practical development of the method.

construction, the contour lines seen through the drop give its isoclinal lines. For the center region, black and white rings were used. For the border region, red and white ones were used. Furthermore, green radial stripes were drawn through the center of the target. These measures allowed for a greater contrast of the photos.

The use of a computer screen, as suggested by Tanner, offers the advantage of a great flexibility in creating new patterns. Since the distance between the plate and the image was maintained at 10 cm and since for drops with contact angles of  $90^\circ$ , the target must have a radius of about 20 cm, no currently available computer monitor could be used. That is why in the experimental unit, the image was drawn on a cardboard. Another advantage was that it is not curved like a monitor screen, so that it does not introduce supplemental aberrations. Furthermore, such a target can be easily removed and replaced. That is certainly not the case for a monitor. Of course, an external light source was to be used. A 400 W HPI lamp, used for lighting in horticulture, was used. Because of the high light intensity of this lamp, the shutter time of the camera could be reduced to acceptable values. (See below.) This was not possible when a computer monitor was used.

**3.3.1.2. Plate and Drop Forming.** — A small frame of about  $20\text{ cm} \times 7\text{ cm}$  was mounted on a lab jack, so that it could be displaced in two directions, perpendicular to the optical axis. On the frame, a glass plate or a PE film could be mounted.

Drops were formed by spraying water on the plate or the film. Of course, the geometry of drops, formed in such a “rough” way, not necessarily corresponds to the geometry of a drop, formed by the “gentle” process of condensation. For the development of the method, however, this does not matter.

**3.3.1.3. Camera.** — An ordinary  $24 \times 36$  TTL camera was used. In order to obtain satisfying enlargements, it was equipped with a bellow, commonly used in macrophotography. A 35 mm lens was mounted in the reversed position on the bellow. In this way, magnifications between 2.7 and 5.3 could be obtained. The object distance of the camera was set at infinity.

A calibration of the enlargement factor as a function of the position of the bellow was carried out by comparing the linear dimension of a test card mounted on the sample frame to its image dimension.

The optimal shutter time was determined experimentally. For a film with a sensitivity of 100 ISO, shutter times between  $1/60$  and  $1/15$  of a second seemed to produce the best results. In this way, even for these relatively large magnifications, sharp photographs could be obtained.

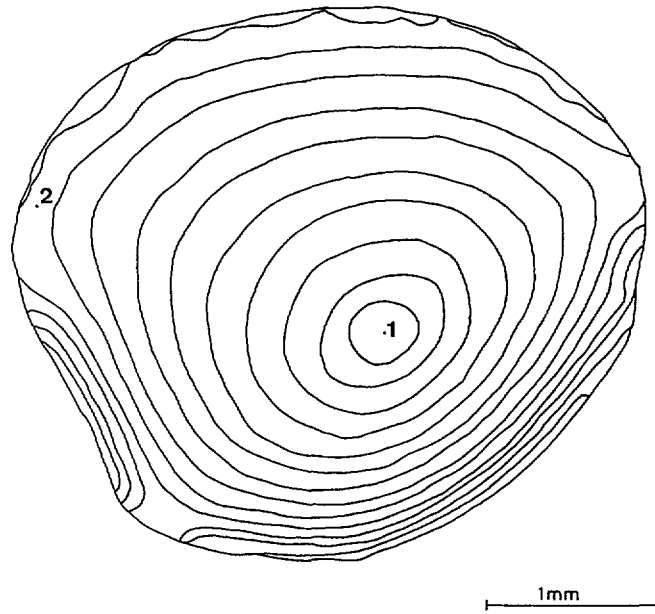


Fig. 4. — Ring contour lines of the target as deformed by the drop in Figure 6 (1: center of the target, seen through the drop; 2: center of the target, seen directly).

3.3.2. *Digitization of the Photos.* — Photos of  $15\text{ cm} \times 10\text{ cm}$  were developed in the commercial circuit. By means of a copier, the drop images were then enlarged to between twice and four times their original size. The target image formed by the drop was then traced on a transparent paper, laid over the copy. At the same time, the center of the target seen through the drop and the directly seen center (optical axis) were indicated on the pattern. Figure 4 gives the result for a water drop on a vertical PE film, obtained in the way described above.

The transparent paper was then placed on a digitizer. Under it lay a paper sheet with 18 radial lines, whose center coincided with the center of the target seen through the drop. Some of these lines are given by the thin dashed lines of Figure 5. Along each of these 18 lines, the intersection points with the isoclinical lines of the drop were digitized. Finally the drop edge was digitized. The information about the point location and the ring number was then stored in a file in such a way that it could directly be treated by the other programs for the calculation of the drop height in each point.

3.3.3. *Calculation of the Drop Shape.* — By means of the equations (10), (14) and (17), together with the correction for off-alignment mentioned in paragraph 3.2.2, the drop height could be calculated for all points along the radial lines. However, the rigorous introduction of this correction required that the position of the top of the drop is known and that the digitization of the contour lines of the projected rings is carried out with reference to this point. Normally this point cannot easily be found. For the drop of Figure 4, it is of course situated on the line through the points 1 and 2. As it cannot easily and exactly be found, a trial and error method is needed. Of course, the use of the correction formulas would then require to restart the digitization for each attempt. That is why another approximative, though easy-to-use method was adopted.

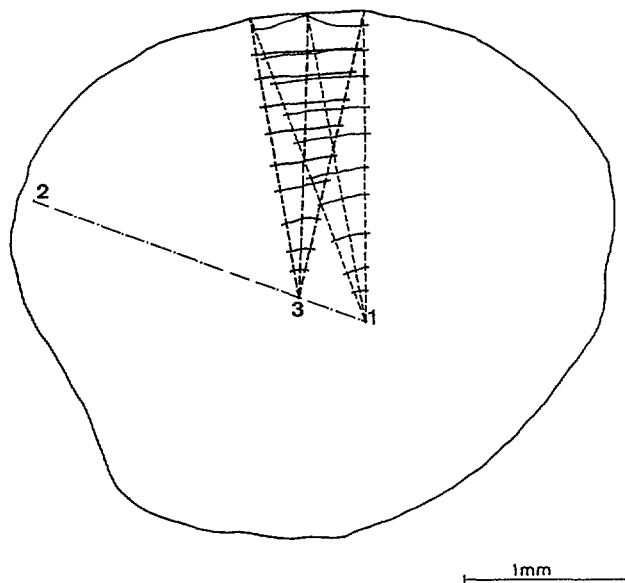


Fig. 5. — Ring contour lines before (thin) and after (thick lines) correction for a small part of the drop of Figure 4.

Figure 5 partly shows the isoclinal lines (thin unbroken lines) for the drop of Figure 4. This deformed pattern was “corrected” in the following way. A point 3 on the line 1-2, supposed to be the actual drop maximum, was chosen as the new reference point. The radii along which the digitization had been carried out (thin dashed lines) were supposed to behave like elastics while thrown to the new reference point; *i.e.* the distance from the edge of each point on the new “radius” (thick dashed lines) was obtained by taking its distance from the edge on the old radius and multiplying it by the ratio of the lengths of the respective radii. In this way, the corrected isoclinal lines could be obtained (thick unbroken lines). As the corrections are usually small, the errors introduced here are also small.

For the “corrected” configuration, the height of the drop top was calculated by application of equation (17), starting from the border of several radial planes. By trial and error, this procedure was restarted for several locations of the supposed drop maximum (point 3), till the maximum drop heights, calculated in the several radial planes satisfactorily coincided.

The unavoidable small errors between the drop heights, calculated in the several radial planes, were then eliminated by forcing the height of the drop to equal the mean value of the calculated heights at the top of the drop and by correcting the intermediate heights.

The transformation of the isoclinal network into a contour line pattern was completely automatized, so that a relief map of the drop could be drawn. (See Fig. 6.) The interpolation results of this program were then transformed to a file format that can be read by the light transmission simulation programs described in [9].

**3.4. ASSESSMENT OF THE METHOD.** — According to Figure 6, the method can certainly be considered as satisfying. The above described method is undoubtedly cheap. Photographs can be taken very quickly, so that evaporation or condensation will not considerably influence the form of the drops during the procedure, even if the heat produced by the lamp cannot directly be evacuated. The materials and apparatus are light and easy to move.

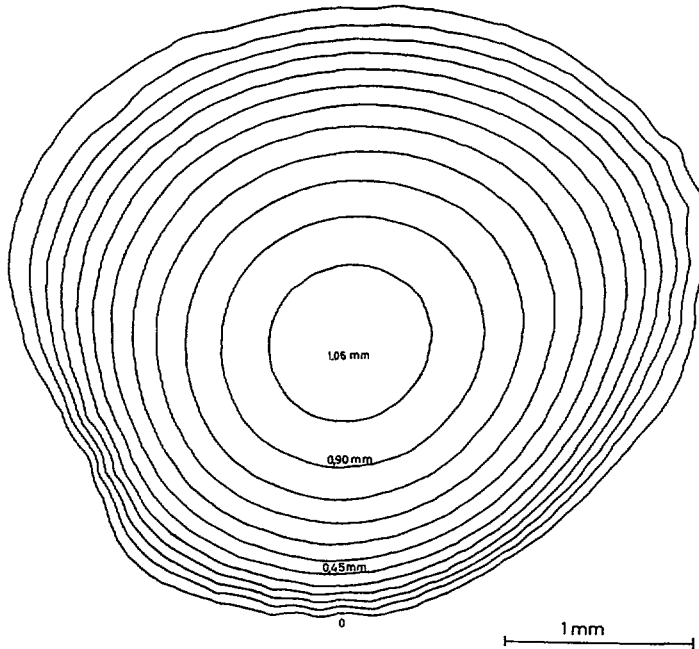


Fig. 6. — Relief map of the drop after correction.

Yet the method has a few disadvantages. If the photographs are not very sharp, the results can be influenced by human interpretation during the tracing of the contour lines of the rings. It was tried to eliminate this problem by using a scanner. However, it was observed that a standard scanner was not able to discern the contour lines for all points of the photograph. This also implies another disadvantage of the method: its labourintensity. Use of a high quality scanner and software could probably eliminate this problem.

#### 4. Simulations of Light Transmission for Experimentally Determined Drop Geometries

##### 4.1. LIGHT TRANSMITTANCE

**4.1.1. Sprayed Drops.** — Photographs for the determination of real drop geometries were again taken by spraying drops on a vertical PE film, just like described in paragraph 3.3.1.2. A series of 15 drops on a vertical PE film was treated in the way described in paragraph 3. Very different drop geometries have been taken into account.

For the simulation of light transmittance and diffusion through drops, a program described in [9], was used. In this program, parallel light rays of unit flux are supposed to strike a slab or plastic film, covered by a liquid drop, at its external dry surface. After refraction at both surfaces of the covering material and possibly after multiple reflections inside the covering material, the rays enter the drop. Here again they are refracted and reflected in different rays with lower fluxes, which are stored in a kind of database. The extinction of the rays by absorption in the cladding material and in the water is taken into account for each step of the simulation. The fluxes of the rays leaving the drop at the water-air interface are summed. By

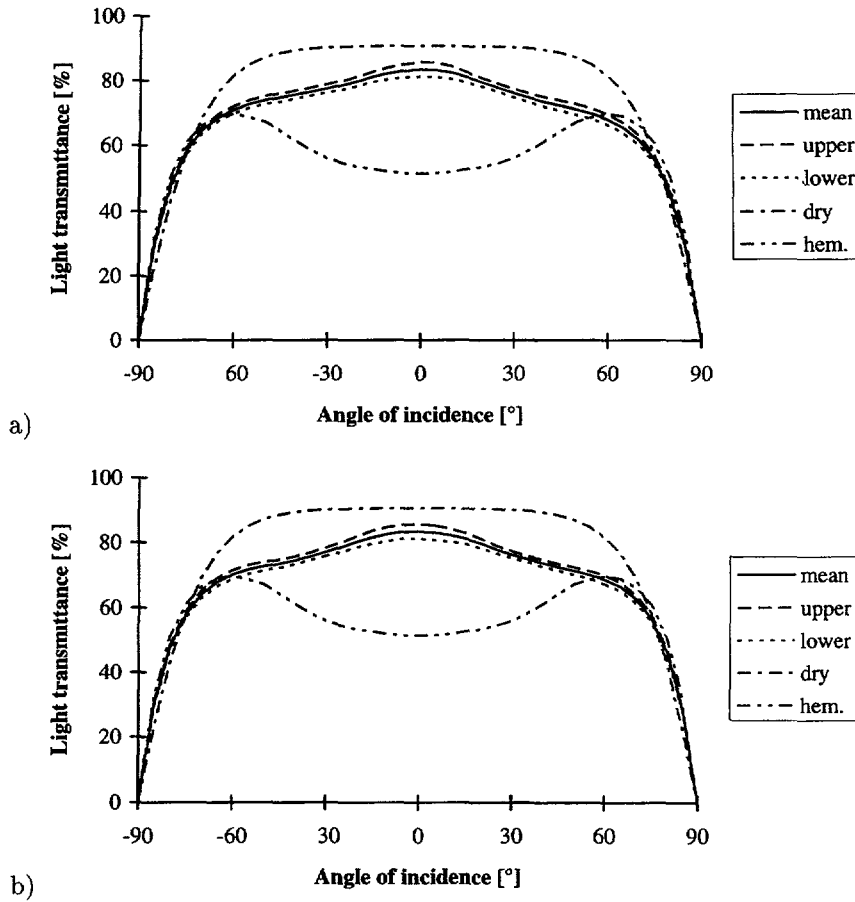


Fig. 7. — Light transmittance curves for a (“dry”) dry PE film, for a (“hem.”) hemispherical drop on a PE film and for experimentally determined drops on a vertical PE film (mean value, together with the upper and lower limits of the 95% confidence interval) for incident light rays parallel to the a) vertical and b) horizontal planes through the center of the drops.

dividing this sum by the amount of unit flux rays, originally striking the slab at the dry side, the light transmittance can be calculated. At the same time, the directions of the rays leaving the drop, are stored, allowing for the study of the scattering effect.

In this way, light transmittance curves were then simulated for light incidence planes parallel to the vertical ( $xz$ ) and the horizontal ( $yz$ ) planes through the top of the drop. Figures 7a and 7b give the simulated transmittance curves for light rays in the vertical and horizontal planes. For the 15 drops, the average light transmittance is given, together with the 95% confidence interval. It can be concluded that despite the very different geometries, the confidence interval for the mean light transmittance is very small. Because of the specific wettability of PE films, which results in rather flat drops, the transmittance curves diverge from the one for a hemispherical drop and they get closer to the curve for a dry PE film. Furthermore, it can be observed that for light incidence in a vertical plane (See Fig. 7a), a slight asymmetry is observed: for the zone of higher advancing contact angles (positive incidence angles), the light transmittance is somewhat lower.

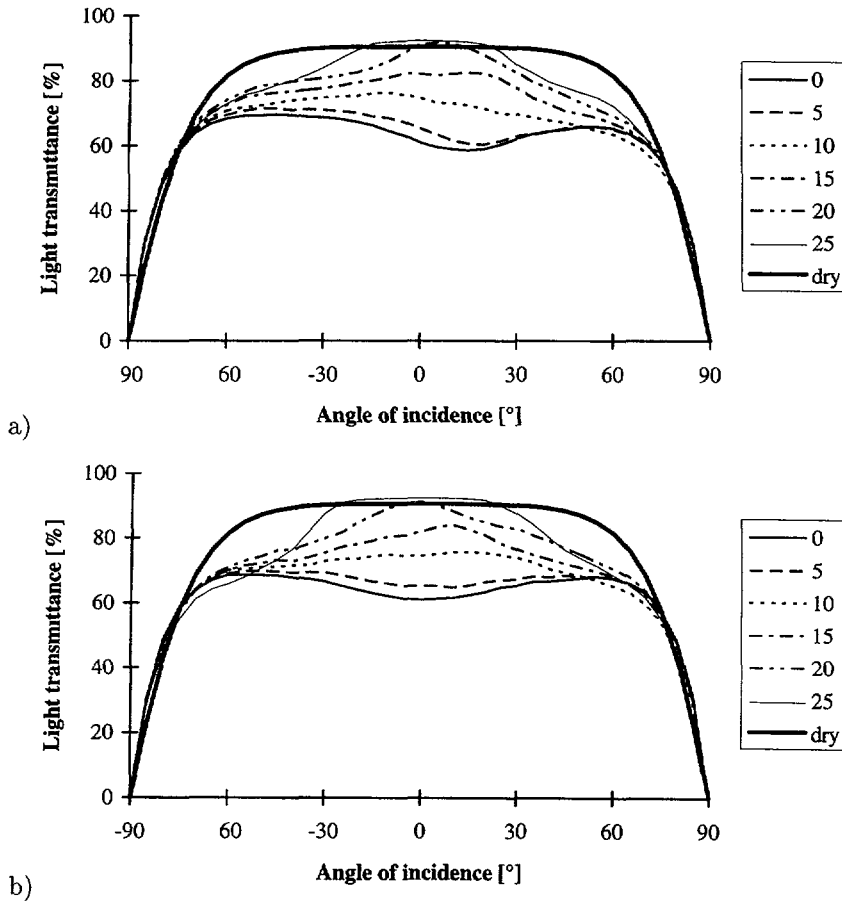


Fig. 8. — Light transmittance curves for a (“dry”) dry PE film and for experimentally determined geometries of an evaporating drop (time in minutes) on a vertical PE film for incident light rays parallel to the a) vertical and b) horizontal planes through the center of the drop.

4.1.2. *Evolution of Drop Shape and Light Transmittance During Evaporation.* — To study the influence of evaporation on the light transmittance, photographs of a same drop were taken at 5 minutes intervals. The drop geometry was followed during 25 minutes. It was found that during evaporation, the drop first flattens and only at the end of the evaporation process, the water-PE interfacial area decreases. The drop geometries were again used as input for the simulation program.

Figures 8a and 8b give for each single drop geometry the simulated transmittance curves for light rays in the vertical and horizontal planes. It can be observed that the flatter the drops, the more light is transmitted in the zone of low incidence angles. This is in total agreement with the conclusions drawn by [9] for cap shaped drops. It can also be concluded that only for very flat drops and at nearly normal incidence, the light transmittance can be higher than for the dry film. Figure 8a for the vertical plane clearly reveals that the skewness of the transmittance curves depends on the contact angles: bigger drops with a more important difference between their advancing and receding contact angles give rise to more asymmetric curves.

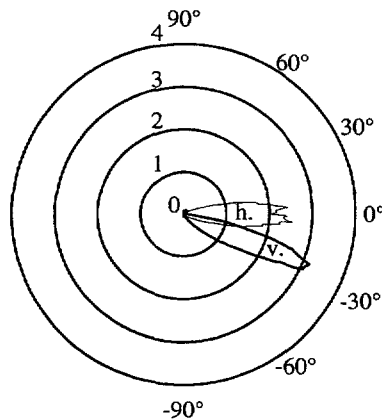


Fig. 9. — Mean light diffusion indicators projected in the (“v.”) vertical and (“h.”) horizontal planes through the center of the experimentally determined drops.

4.2. LIGHT DIFFUSION. — Light diffusion was simulated for all 21 reconstructed drop geometries in the way described by [9]. Light was supposed to incidence in the vertical plane perpendicular to the PE film. The angle of incidence was supposed to be  $30^\circ$  above the horizontal plane. The results for the several drops were then averaged, so that one set of diffusion indicators was obtained for the whole series. Figure 9 shows these diffusion indicators, representing what part of the total entering light flux leaves the drop in a certain direction, projected on a horizontal and on a vertical plane. (To obtain very smooth indicators, enormous amounts of calculations are necessary. As the conclusions to be drawn are not altered by the smoothness, these rough indicators suffice for this study.) Direction classes of  $1^\circ$  were used so that the diffusion indicators are expressed in % light transmittance per  $^\circ$ . From this figure and from the numerical results, it can be concluded that the maximum in the vertical plane is always found for  $-22^\circ$  and that the drop shape has hardly any influence on the diffusion indicators. For flat drops as well as for strongly curved drops, nearly all the light is diffused in a small solid angle around the direction of the light rays entering the drop at the film-water interface, just like for hemispherical drops, as demonstrated in reference [9].

## 5. Summary and Conclusions

A method allowing for the numerical determination of the geometry of real drops on transparent materials was developed. Correction techniques for deviations of the optimal conditions were also given. The method revealed to be rather quick, although labourintensive. Furthermore, as only instruments that are currently available in laboratories are used, the method is very cheap. Use of more performing instruments, such as high quality scanners, cameras, . . would reduce the labour charge and allow for even better results (*e.g.* for very small drops) but would also increase the costs.

By means of this method, the drop geometries of a series of 15 drops, sprayed on a vertical PE film, were determined and then input in a program for the simulation of light transmission and light diffusion. It was shown that the light transmittance of these flat drops was somewhat lower than the light transmittance for dry PE but much higher than for hemispherical drops. Light diffusion was shown to be nearly independent of drop shape, nearly all the light being

diffused in a small solid angle around the direction of the light rays entering the drop at the PE-water interface.

By means of the same method, the geometry of an evaporating drop on a vertical PE film was determined at 5 minutes intervals. It was found that during evaporation, the drop flattens before shrinking. As a consequence, the light transmittance curve for a fresh drop looks more like the one of a hemispherical drop and evolves during evaporation towards the curve for a water film of constant thickness.

## Annex

### Estimation of the theoretical error for non symmetric drops

As an example, the error made by using equation (12) instead of equation (18) for asymmetric drops will be estimated for a light ray leaving a drop, having the shape of half an ellipsoid with equation ( $x$ ,  $y$  and  $z$  in mm)

$$\frac{x^2}{4} + \frac{y^2}{9} + \frac{z^2}{4} - 1 = 0 \quad (\text{A.1})$$

at the point with coordinates (1;1;1.60). For this ellipsoid, the excentricity is 1.5, which is rather high, certainly for drops formed by condensation. For this specific situation, the angle  $\gamma$  between the plane containing the axis through the center of the target and through the top of the drop and the plane containing the incident and the outgoing light ray at the point where the light ray leaves the drop, is about  $21^\circ$ . Calculating the slope angle  $\eta$ , which is found to be  $34^\circ$ , then allows for the calculation of  $l_2$  by application of equations (10) and (14), in which  $R + r_e$  are replaced with  $l_2$ . For the above described drop on a PE film with a thickness of 0.1 mm and with a refractive index of 1.515, and supposing a target-drop distance of 100 mm,  $l_2$  is found to be 22.39 mm. By means of equation (18),  $R$  is then found to be 21.08 mm or about 15 times the length of  $r_e$  (1.414 mm).

If equation (12) were used for the calculations,  $l_2$  would be calculated as  $R + r_e$  or 22.49 mm. This implies that even for relatively important values of  $\gamma$ , the error on  $l_2$  is still smaller than 0.5%. It is clear that the error will even be smaller if the distance between the target and the drop  $l_1$  is increased, since in that case  $R$  will also increase for the same configuration. It can thus be stated that the errors for asymmetric drops can always be kept negligible.

## References

- [1] Merte H., in: "Condensation heat transfer", Irvine T.F. and Hartnett J.P., Eds., Advances in heat transfer, part 9. (Academic Press, New York, 1973) pp. 181-272.
- [2] de Gennes P.G., Wetting: statics and dynamics, *Rev. Mod. Phys.* **57** (1985) 827-863.
- [3] Larkin B.K., Numerical solution of the equation of capillarity, *J. Colloid Interface Sci.* **23** (1965) 305-312.
- [4] Novick-Cohen A., On a minimization problem arising in wetting, *SIAM J. Appl. Math.* **52** (1992) 593-613.
- [5] Merte H. and Yamali C., Profile and departure size of condensation drops on vertical surfaces, *Wärme -und Stoffübertragung* **17** (1983) 171-180.

- [6] Bracke M., De Bisschop F. and Joos P., Contact angle hysteresis due to surface roughness, *Progr. Colloid Polym. Sci.* **76** (1988) 251-259.
- [7] Tanner L.H., The form and motion of draining oil drops, *J. Phys. D: Appl. Phys.* **18** (1985) 1311-1326.
- [8] Tanner L.H., A study of liquid drop lenses using a deflection mapping technique with extreme angular range, *J. Opt. Laser Technol.* **20** (1988) 149-155.
- [9] Pieters J., Deltour J. and Debruyckere M., Light transmission through condensation on glass and polyethylene, Accepted for publication in *Agric. Meteorol.* (1996).